The momentum balance of steady flow past an island

R C Musgrave and T Peacock

Massachusetts Institute of Technology
rmusg@mit.edu

Abstract

The interaction of large-scale ocean currents with tall topography generates phenomena from turbulence at the smallest scales, to lee waves and quasi-geostrophic eddies at the largest. We investigate the role of such processes in setting the momentum balance downstream of an island in an idealized, three-dimensional numerical simulation. Our parameter regime is inspired by conditions close to Palau in the western Pacific, where the North Equatorial Current is incident on the meridionally oriented island and Mariana Ridge. In our highly idealized setup, a strong, shallow, meridionally tilted thermocline supporting a zonal geostrophic surface flow encounters a tall, meridionally elongated island. Pressure gradients are setup around the ridge which drive both ageostrophic and geostrophic processes, extracting and redistributing momentum from the background flow.

1 Introduction

The classical problem of unstratified flow past a bluff body is associated with a range of processes, including boundary layer formation, flow separation, vortex shedding and form drag (Kundu et al., 2012). In the ocean, flow past islands gives rise to qualitatively similar processes, but it is modified by planetary rotation, stratification, non-uniform flows and irregular bathymetry. Island wakes in the lee of a cylindrical island were considered in a comprehensive study by Dong et al. (2007), who found that flows are sensitive to three nondimensional parameters: the Reynolds number (Re), Rossby number (Ro) and the Burger number (Bu). As for homogeneous flows, wake eddies are attached for low Reynolds numbers, and form a von Kármán vortex street for high Reynolds numbers. However, stratification and rotation cause the evolution of the wake to differ from the homogeneous case, with the appearance of centrifugal, barotropic and baroclinic instabilities downstream.

The influence of topography on the large scale circulation is mediated by such processes, which redistribute the momentum of the overlying flow. In addition to triggering wake eddies, islands in the ocean have submerged flanks which can generate lee waves. In the atmosphere, lee waves alter the mean flow by transporting momentum away from topography and depositing it where they dissipate (Bretherton, 1969).

In this idealized numerical study, we begin to relate the effects of islands to the larger scale wind driven circulation of the subtropical gyres by examining their influence on momentum pathways. The subtropical gyres are commonly assumed to be in Sverdrup balance, which means that the momentum input by the wind is balanced by lateral viscosity at strong western boundary currents. This linear theory assumes a flat ocean bottom, and though it appears to explain the largest scale flows, evidence of this balance in the real ocean has not been established (Wunsch and Roemmich, 1985). In contrast to the gyres, the Antarctic Circumpolar Current is thought to be in a different balance, with the momentum input by the windstress balanced by bottom pressure against topography. We are interested in the importance of both form drag and nonlinear processes arising

from the interaction of the wind driven circulation with tall topography on the overall gyre circulations.

Our parameter regime is similar to that of the island Palau, located along the Marianas Ridge in the western Pacific. At this location, the geostrophically balanced westward North Equatorial Current (NEC) forms the southern branch of the subtropical gyre, flowing past the island in the upper 500m. Our focus on this region is motivated by a large field experiment taking place in 2016-17. For the stratification, we estimate that the baroclinic Rossby radius, $L_r = 130$km. The Burger number, $\mathrm{Bu} = (L_r/D)^2 \approx 3.5$ where D is the meridional lengthscale of the island (we take to be 70km), and the Rossby number, $\mathrm{Ro} = U/fD \approx 1$, where f is the coriolis frequency, and U is the strength of the NEC.

2 Model setup

The simulation is performed using the MITgcm (Marshall et al., 1997), a finite-volume Navier-Stokes, hydrostatic, Boussinesq model. We initialize the simulation with a meridional temperature gradient extracted from the Roemmich-Gilson ARGO climatology at 8°N and 133°W (Roemmich and Gilson, 2009). The initial zonal flow is in geostrophic balance with the temperature gradient, with a peak of about -0.4 ms^{-1} at the surface, decaying over the upper 400m (Figure 1b.). An isolated island is located about two-thirds along the channel, with length scales comparable to Palau (see Figure 1a.).

The model solves the following discretized equations:

$$\frac{\partial u}{\partial t} + \mathbf{u}\cdot\nabla u - fv = -\frac{\partial p}{\partial x} + \nu_H\nabla_H^2 u + \nu_V\frac{\partial^2 u}{\partial z^2} + \mathcal{F}_u \tag{1}$$

$$\frac{\partial v}{\partial t} + \mathbf{u}\cdot\nabla v + fu = -\frac{\partial p}{\partial y} + \nu_H\nabla_H^2 v + \nu_V\frac{\partial^2 v}{\partial z^2} + \mathcal{F}_v \tag{2}$$

$$\frac{\partial w}{\partial t} + \mathbf{u}\cdot\nabla w = -\frac{\partial p}{\partial z} + b + \nu_H\nabla_H^2 w + \nu_V\frac{\partial^2 w}{\partial z^2} \tag{3}$$

$$\frac{\partial b}{\partial t} + \mathbf{u}\cdot\nabla b + N^2 w = \kappa_H\nabla_H^2 b + \kappa_V\frac{\partial^2 b}{\partial z^2} + \mathcal{F}_b \tag{4}$$

$$u_x + v_y + w_z = 0. \tag{5}$$

We employ eddy diffusivities and viscosities (κ_H, κ_v, ν_H and ν_v) to maintain stability, and increase the vertical viscosity and diffusivity coefficients in overturns in an energetically consistent manner (Klymak and Legg, 2010). We choose an eddy viscosity of 5 $\mathrm{m}^2\mathrm{s}^{-1}$ for stability, but its large value is justified as an oceanic flow is expected to be fully turbulent. Our Reynolds number, $\mathrm{Re} = UD/\nu_e = 2\times10^4$. Resolutions in the interior are $dx = dy = 500$m, with a vertical resolution of 5 m at the surface, and 80 m at the bottom. The grid is telescoped in the outer 186 grid-points in both the zonal and meridional directions, and the flow in these regions is sponged back to the initial geostrophic flow, damping baroclinic features without reflecting them back into the interior.

2.1 Analysis framework

We split the flow into a time mean and time dependent component, for example $u = \langle u\rangle + u'$, then form the time averaged equations. The time mean zonal momentum equation becomes:

$$(\langle u'u'\rangle_x + \langle u'v'\rangle_y + \langle w'u'\rangle_z + \langle u\rangle\langle u\rangle_x + \langle v\rangle\langle u\rangle_y + \langle w\rangle\langle u\rangle_z) - f\langle v\rangle = -\langle p\rangle_x + \nu\nabla^2\langle u\rangle \tag{6}$$

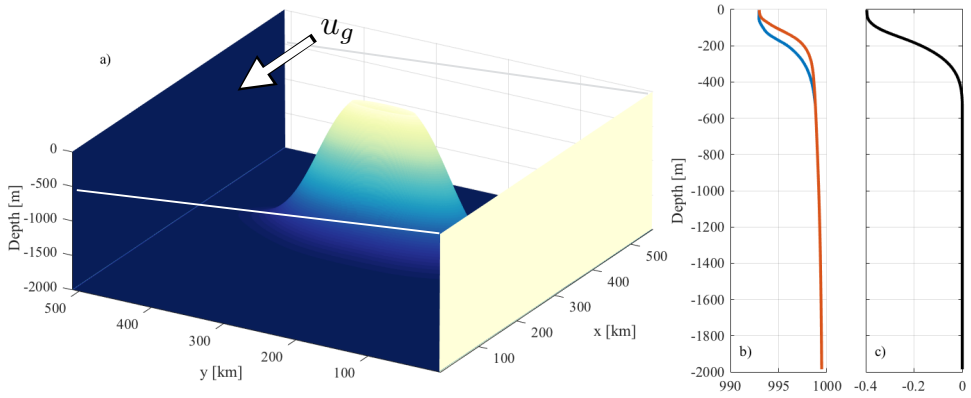

Figure 1: a) A meridionally oriented island is centered in a channel, with walls to the north and south. A surface confined, geostrophically balance westward flow interacts with the topography. b) Density profiles from the north (blue) and south (red) of the domain. c) Zonal velocity profile in geostrophic balance with a linearly interpolated density profiles from b.

The advective terms are now written in terms of the divergences of momentum fluxes: the Reynolds stresses (for example $\langle u'v' \rangle_y$) arise from time dependent (eddy) processes, and the time mean advection of momentum is captured in the mean fluxes (for example $\langle u \rangle \langle v \rangle_y$). Divergent Reynolds stresses exert a force on the fluid, and in this simulation form an important component of the ageostrophic balance.

The role of topography is often discussed in terms of form drag,

$$F_D = \int_x \langle p(-h) \rangle h_x \, dx', \tag{7}$$

which arises from the pressure term in the volume integral of equation (7). For isolated topography where the flow returns to an identical "background" far upstream and downstream, this is the full integral of the term $\langle p \rangle_x$ which is balanced by the pressure drop across the topography. Here we follow Masich et al. (2015), concentrating on the pressure drop across the topography, though cognizant that in an ocean basin with walls at the zonal extent, the pressure drop may include a large scale basin response that is not typically referred to as form drag.

3 Results

3.1 Qualitative description of flow

During the initial transient period, fast, full depth propagating modes radiate horizontally from the topography, setting the upstream and downstream conditions (Baines and Hoinka, 1985). The initial flow diverges around the island, generating layers of intense cyclonic vorticity to the north and anti-cyclonic vorticity to the south. By 150 hr after the start of the simulation, a pair of counter-rotating vortices have formed with the anticyclonic vorticity further downstream, and the cyclonic vorticity exhibiting instabilities along the strong shear layer.

The flow downstream of the island forms a low frequency von Kármán street, shedding alternate eddies with a period of around 15 days. The inclusion of rotation leads to differences in the evolution of the the cyclonic (north) and anticyclonic (south) vorticity,

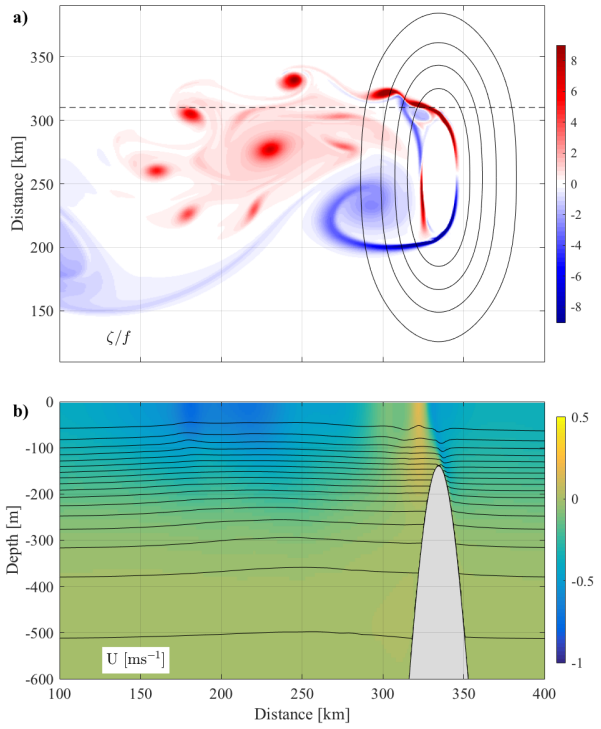

Figure 2: Snapshot of the flow 15 days after the start of the simulation. a) Surface vorticity normalized by the Coriolis frequency, showing the asymmetric generation of cyclonic and anticyclonic vorticity at the northern and southern edges of the island; b) A zonal slice across the submerged northern flank of the island showing zonal velocity (colors) and isopycnals (contoured). The downstream slanted feature at the crest of the ridge fluxes westward zonal momentum upwards.

with the large cyclonic shears at the northern tip of the island rolling up in shear instabilities, which form a ring of small vortices around the larger recirculation in the lee of the island (Figure 2). Conversely, the anticyclonic vorticity at the southern tip is more stable to shear instabilities, but is susceptible to centrifugal instability as $|\zeta|/f$ is large, and is generally less intense than the cyclonic vorticity.

The passage of a steady flow over a two-dimensional, submerged ridge will generate lee waves, extracting momentum from the fluid at depth and fluxing it upwards towards the surface. However, it is unclear to what extent lee waves are important in steady flows over three-dimensional objects, where the fluid can pass around, instead of over, the topography. Figure 2b shows a zonal slice through the flow at $y = 305$km (marked by a dashed line in 2a), a location where lee waves may be expected to form over the flanks of the island. A sloped feature above the crest of the ridge ($x = 340$km) is tilted downstream, in contrast to that expected for lee waves in an unsheared flow, whose wave crests advance upstream with height. The feature is associated with the sharp surface vorticity signature at flow separation, and has $\langle uw \rangle < 0$ (not shown), indicating that it fluxes westward momentum upwards, enhancing the surface westward flow downstream.

3.2 The time mean flow

We evaluate the terms of Equation (7) over 240-478 hr of the simulation, then average over the upper 500m. Unsurprisingly, to leading order the flow is geostrophically balanced,

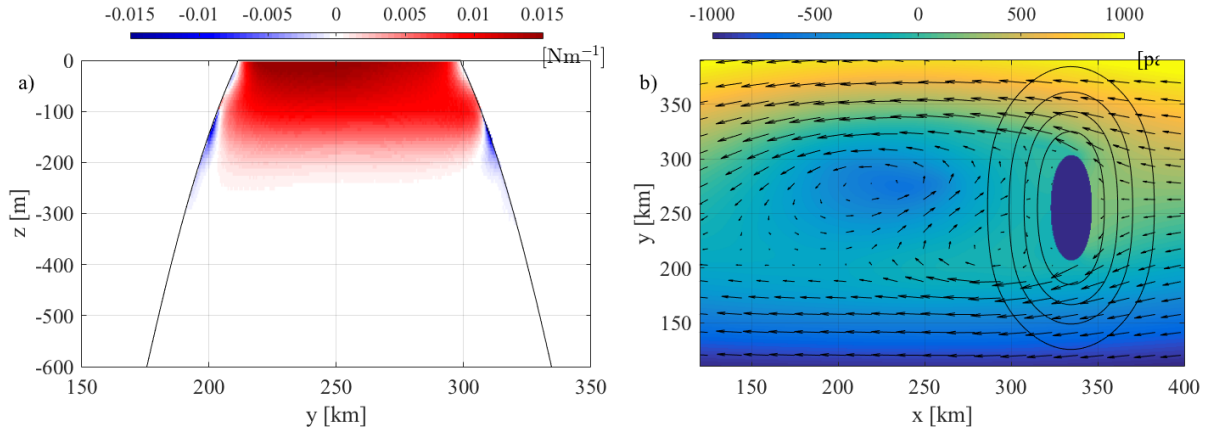

Figure 3: a) Distribution of form drag exerted by the topography on the flow b) Mean pressure and velocity at 50m. Flows are geostrophic to leading order and form a pair of eddies, time mean cyclonic vorticity to the north, and anticyclonic to the south.

with $\langle p \rangle_x \approx f \langle v \rangle$, an order of magnitude greater than the other terms. The geostrophic flow is composed of a pair of eddies in the lee, associated with cyclonic vorticity to the north, and anticyclonic vorticity to the south (Figure 3b). The eddy pair is asymmetric, with the cyclonic eddy being larger and stronger in the mean than the anticyclonic.

Ageostrophic flows are supported by the nonlinear terms, of which the most important are the horizontal advection of momentum by both the eddy (e.g. $\langle u'v' \rangle$) and the time mean terms (e.g. $\langle u \rangle \langle v \rangle$). In Figure 4 we show the eddy and time mean advection of zonal momentum by the meridional flow at $x = 300$km. Both eddy and time mean fluxes are equally important, with regions of negative $\langle u'v' \rangle_y$ imposing a positive zonal force on the flow directly behind the topography, and positive $\langle u'v' \rangle_y$ imposing a negative zonal force in the regions of the separated jets. On the outer flanks of the jets, the mean fluxes dominate, slowing the strong westward jets. The separation of the westward surface flow

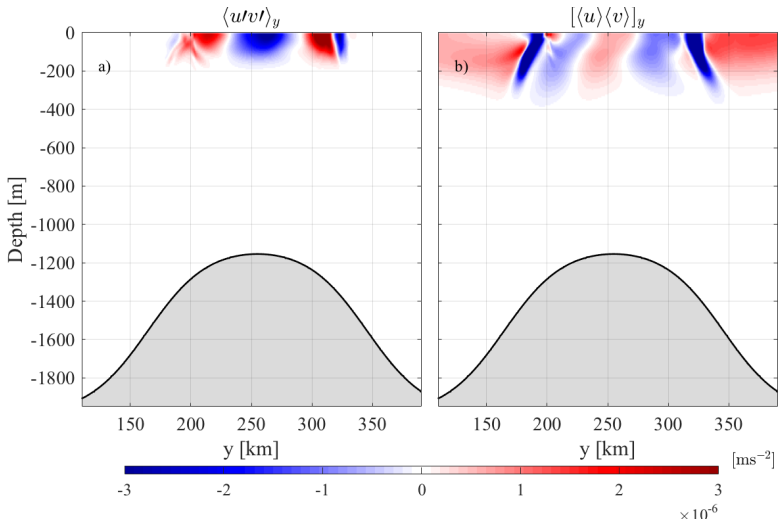

Figure 4: Nonlinear terms in the zonal momentum equation. a) eddy fluxes transfer westward momentum to the north and south, depositing it in the jets; b) the mean advection of momentum transfers dominate in the jets, removing westward momentum.

at the meridional extent of the island leads to a large pressure drops corresponding to

more than 3mm of sea surface height over the island, and we show the time mean form drag in Figure 3a. Close to the northern and southern tips of the island the form drag drops as the downstream pressure deficit is small in the region where the boundary layer separates. Below 100 m, relatively high pressures downstream are associated with time mean eddies close to the separation point, which increase the adverse pressure gradient encountered by the boundary flow over that expected in an unstratified flow, causing the form drag to reverse in these narrow regions.

3.3 Boundary current separation

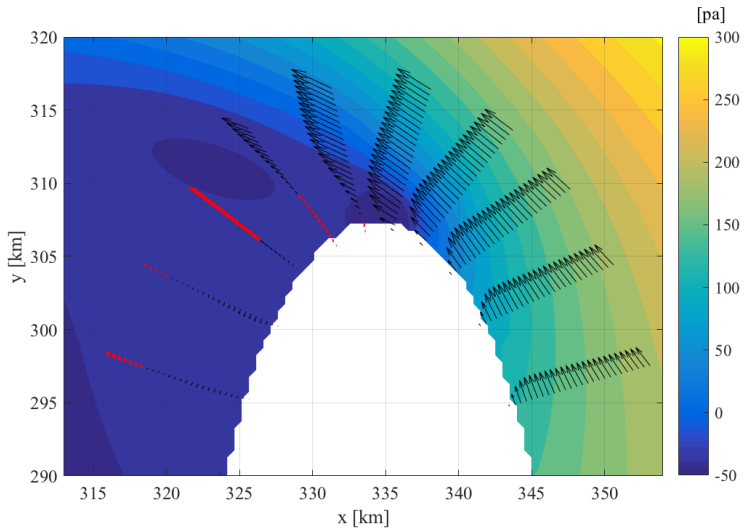

Figure 5: Time mean boundary flow (vectors) at $z = 100$m. Red vectors indicate reversed flow. Colors show time mean pressure anomaly with respect to mean upstream pressure at $z = 100$m.

The enhanced westward flow separates from the topography at the northern and southern tips of the topography, forming a strongly sheared layer which forms the wake eddies downstream. As in the classical boundary layer problem, the momentum balance at the boundary is between the pressure gradient and viscosity. Upstream of the object, a favorable pressure gradient ($\frac{\partial p}{\partial x} > 0$) causes the flow to parallel the isobath. At the tip of the island, in a manner analogous to classical unstratified flow past a bluff body, separation occurs where the pressure gradient along the isobath reverses direction, forming an adverse pressure gradient (Kundu et al., 2012). At this point the velocity profile develops an inflection as

$$\nu_H \left(\frac{\partial^2 u}{\partial y^2} \right) = \frac{\partial p}{\partial x} < 0, \tag{8}$$

where the coordinate is rotated to be parallel and perpendicular to the boundary. Reversed flow forms between the topography and the boundary layer (Figure 5 in red), and the layer separates.

4 Summary

We have presented some aspects of the zonal momentum balance associated with the flow of a surface intensified current such as the NEC past an idealized island at 8°N. The geostrophically balanced westward surface flow separates from the topography near its meridional extents, forming strongly sheared boundary layer currents downstream of separation. Eddies of alternate sign form in the lee of the island forming a von Kármán vortex street which are dominantly geostrophic, with periods of around 15 days. In contrast to the anticyclonic shear to the south of the island, instabilities in the cyclonic shear to the north lead to a train of small eddies, which wrap around the cyclonic "island" scale eddies of the vortex street. Flow separation leads to a significant form drag by the island on the overlying flow, with pressure drops corresponding to greater than 3mm of sea surface height.

Though the incident flow is steady, the flow downstream is not, and eddy fluxes are an important mechanism for the redistribution of momentum in the lee. Eddy fluxes dominate the mean advection of momentum in the lee of the island, imposing a positive zonal force on the flow. The boundary layer jets are enhanced by eddy fluxes, and opposed by time mean advection.

References

Baines, P. G. and Hoinka, K. (1985). Stratified flow over two-dimensional topography in fluid of infinite depth: A laboratory simulation. *Journal of Atmospheric Sciences*, 42(15):1614–1630.

Bretherton, F. (1969). Momentum transport by gravity waves. *Quarterly Journal of the Royal Meteorological Society*, 95(404):1–31.

Dong, C., McWilliams, J. C., and Shchepetkin, A. F. (2007). Island Wakes in Deep Water. *Journal of Physical Oceanography*, 37(4):962–981.

Klymak, J. and Legg, S. (2010). A simple mixing scheme for models that resolve breaking internal waves. *Ocean Modelling*, 33(3-4):224–234.

Kundu, P., Cohen, I., and Dowling, D. R. (2012). *Fluid Mechanics*. Elsevier, 5th edition.

Marshall, J., Adcroft, A., Hill, C., Perelman, L., and Heisey, C. (1997). A finite volume, incompressible Navier Stokes model for studies of the ocean on parallel computers. *Journal of Geophysical Research: Oceans (1978–2012)*, 102(C3):5753–5766.

Masich, J., Chereskin, T., and Mazloff, M. (2015). Topographic form stress in the Southern Ocean State Estimate. *Journal of Geophysical Research*, 120.

Roemmich, D. and Gilson, J. (2009). Progress in Oceanography. *Progress in Oceanography*, 82(2):81–100.

Wunsch, C. and Roemmich, D. (1985). Is the North Atlantic in Sverdrup Balance? *Journal of Physical Oceanography*, 15:1876–1880.